

# Flatness of the setting Sun

Z. Néda and S. Volkán

*Babeş-Bolyai University, Dept. of Physics, RO-3400, Cluj, Romania*

*E-mail: zneda@phys.ubbcluj.ro*

(Last revised May 28, 2018)

Atmospheric refraction is responsible for the bending of light-rays in the atmosphere. It is a result of the continuous decrease in the refractive index of the air as a function of altitude. A well-known consequence of this phenomenon is the apparently elliptic shape of the setting or rising Sun (or full-Moon). In the present paper we systematically investigate this phenomenon in a standard atmosphere. Theoretical and numerical calculations are compared with experimental data. The asymmetric rim of the Sun is computed as a function of its inclination angle, observational height and meteorological conditions characterized by pressure, temperature and lapse-rate. We reveal and illustrate some extreme and highly unusual situations.

## I. ATMOSPHERIC REFRACTIONS

Atmospheric refraction is between the first scientifically approached phenomenon. This effect is responsible for the apparent scintillation of stars, mirages, the puzzling and spectacular green flash, difference between apparent and real position of stars or the asymmetric rim of the Sun near the horizon. The refractive index of dry air is very close to 1. Its small dependence on temperature and pressure leads to a refractive index gradient in the atmosphere. Although this gradient is very small, due to the large distances travelled by the light-rays in the atmosphere, it can result observable bending or dispersion.

Atmospheric refraction is usually divided into three categories: astronomical, terrestrial and geodesic. Terrestrial refraction appears when both the object and observer are within the Earth's atmosphere. This refraction is responsible for ordinary mirages, and has been extensively studied [1]. The first one reporting and accounting for mirages was Aristotle in *Meteorologica* [2]. Correctly, he concluded that dense air layers can act as mirrors, and considered this effect responsible for mirages. (A complete historic and bibliographic study of mirages can be found on the splendid web-page of A.T.Young [3].) Geodesic refraction is a special case of terrestrial refraction where both the object and observer are at low altitudes. A well-known example for this is surveying. We speak about astronomical refraction when a terrestrial observer detects ray-bending effects for the light-rays coming from objects outside the Earth's atmosphere. This refraction is responsible for the difference between the real and apparent position of stars near the horizon, the green flash or the asymmetric rim of the setting (or rising) Sun. In the present paper we discuss in detail the flatness of the Sun or full-Moon near the horizon. Particularly, we are interested in the extreme values this flatness can take for standard atmospheric profiles, and the dependence of the flatness on the altitude of the observer and meteorological conditions (temperature and pressure). A similar study, considering fixed atmospheric

conditions was recently published by Thomas and Joseph [4]. Here we plan a more complete analysis, considering three different theoretical methods, experiments, computer simulations and illustration of the results with a collection of pictures and movies.

The spectacular nature of sunset or sunrise makes the phenomenon attractive to students. After our experience it can effectively be used to exemplify refraction phenomena and exercising the principles of geometrical optics. Our paper is structured as follows. First, we introduce the atmosphere model, and the refractive index profile is given. Then, we present three different methods for computing the ray-path in this atmosphere. Results computed for different meteorological conditions and observation altitude will close the theoretical part. Experimentally, we analyze and compare with theory the measured flatness for some sunsets photographed or video-filmed by us. Finally, we discuss some extreme and unusual conditions which are exemplified by pictures and movies on a web-page supporting this study. From this web-page one can also freely download a computer-program written by us, which visualizes the sunset for arbitrary meteorological conditions and observation altitude.

We emphasize here, that our study is restricted to standard atmospheric conditions with smooth temperature and pressure profile. Non-standard, but often encountered atmospheric profiles leads to non-standard distortions of the solar rim, and are not considered within this study.

## II. THE OPTICAL ATMOSPHERE MODEL (REFRACTIVE INDEX AS A FUNCTION OF ALTITUDE)

The atmosphere of the Earth is composed mainly of  $N_2$  (79%) and  $O_2$  (20%), and extends up to a few hundreds kilometer height. The refractive index of air is very close to 1, and depends slightly on its pressure and temperature following Edlen's semi-empirical law [5], valid for

dry air:

$$n = 1 + 10^{-6}(776.2 + 4.36 \times 10^{-8}\nu^2)\frac{P}{T}. \quad (1)$$

In the above formula  $\nu$  is the wave-number of the light in  $cm^{-1}$ ,  $P$  is the pressure in  $kPa$  and  $T$  the temperature in  $K$ . Since the pressure and temperature varies within the atmosphere, we get a refractive index gradient which is responsible for atmospheric refractions. Although the variations in  $n$  are quite small, the large distances travelled by light-rays in the atmosphere makes refraction effects observable and sometimes important.

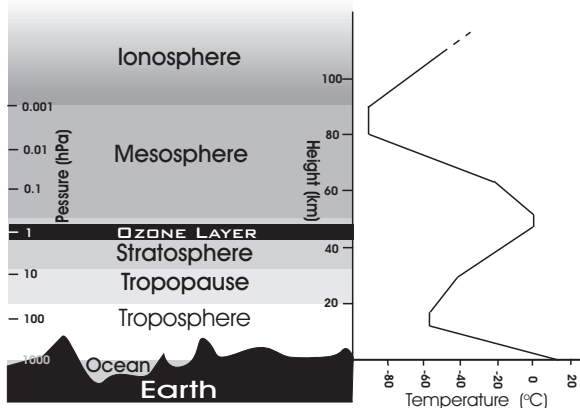


FIG. 1. Distinct layers of the atmosphere, and the standard temperature and pressure profile.

As a function of altitude several layers with different physical properties are distinguishable. The lowest layer extending from sea-level to approximative  $z_t = 14km$  height is called the troposphere. This is the region where the wheatear takes place, i.e. the region of rising and falling packets of air. In this layer the air pressure drops drastically, at the top of the troposphere being only 10% of the value measured at sea-level. In the troposphere the temperature decreases almost linearly with the altitude (Fig. 1). A thin buffer zone between the troposphere and the next layer (the stratosphere) is called the tropopause. Within the tropopause the temperature is in good approximation constant. The stratosphere extends from the altitude of approximately  $18km$  up to  $z_s = 50km$  (Fig. 1). Within the stratosphere the air flow is mostly horizontal. In the upper part of the stratosphere we have the ozone layer. Inside the stratosphere the pressure decreases further with the altitude, but surprisingly the temperature increases with height. Above the stratosphere we find the mesosphere and the ionosphere. In these regions the air is very rare and the temperature profile is shown in Fig. 1.

From the viewpoint of atmospheric refractions only the first two layers, the troposphere and the stratosphere are important. In the upper layers of the atmosphere the air is so rarefied, that the refractive index can be considered 1 within a good approximation.

An accepted and widely used model for the atmosphere

is the U.S. Standard Atmosphere, established in 1953 and re-actualized in 1976 [6]. The U.S. Standard Atmosphere consists of single profiles, representing the idealized steady-state atmosphere for moderate solar activity. The listed parameters include temperature, pressure, density, gravitational acceleration, mean particle speed, mean collision frequency, mean free path, etc. as a function of altitude. In our study we consider an atmosphere model with a spherical symmetry, all relevant physical quantities (temperature and pressure) varying only as a function of altitude. We then calculate the refraction index of air as a function of altitude as follows:

(i) The temperature profile in the troposphere is linearly decreasing with a  $\lambda = 6.5K/km$  lapse-rate, as suggested by the U.S. Standard Atmosphere. Following again the U.S. Standard Atmosphere we consider the temperature constant within the tropopause. Although the temperature increases as a function of altitude in the stratosphere, due to the rarefied air (small pressure) the refractive index is close to 1, and for the sake of simplicity we assume the temperature as constant in this region, too. (We checked that this approximation is fully justified.) Above  $z_s = 50km$  height we assume that the refractive index is 1, and do not calculate it anymore by Edlen's formula. Up to the top of the stratosphere the temperature profile is therefore presumed as

$$T(z) = T_0 - \lambda z \text{ for } z < z_t \quad (2)$$

$$T(z) = T_0 - \lambda z_t \text{ for } z_t \leq z \leq z_s, \quad (3)$$

where  $z$  is the altitude from sea-level, and  $T_0$  the temperature at sea-level.

(ii) For the pressure profile we use a barometric formula in which we take into account the variation of temperature with altitude. Considering a vertical slice of air with thickness  $dz$ , the variation of pressure within this slice is due to the hydrostatic pressure

$$dP = -\rho(z) g(z) dz, \quad (4)$$

where  $g(z)$  is the gravitational acceleration and  $\rho(z)$  the density of air at height  $z$ :

$$\rho(z) = \frac{M}{V} = \frac{Nm}{V} = \frac{P(z)m}{kT(z)}. \quad (5)$$

(We denoted by  $m$  the mass of one molecule,  $N$  the number of molecules in volume  $V$ ,  $T(z)$  the temperature at height  $z$  and  $k$  the Boltzmann constant.) Since we focus on the troposphere and the stratosphere only, the  $z$  height is small in comparison with the radius of the Earth ( $R_E \approx 6378km$ ), thus the  $g$  gravitational acceleration can be considered constant. We can write thus

$$dP = -\frac{P(z)mgdz}{kT(z)}, \quad (6)$$

which is a separable differential equation for  $P(z)$ . Integrating this between a height  $z_0$  where the pressure is  $P_0$

and an arbitrary height  $z$ , we get the desired barometric formula:

$$P(z) = P_0 \exp\left(-\frac{mg}{k} \int_{z_0}^z \frac{dz'}{T(z')}\right). \quad (7)$$

Considering  $z_0 = 0$  (sea-level) and using the temperature profile given by equation (2) and (3) a simple calculus leads us to

$$P(z) = P_0 \left[1 - \frac{\lambda z}{T_0}\right]^{mg/k\lambda} \quad (8)$$

for  $z < z_t$ , and

$$P(z) = P_0 \left[1 - \frac{\lambda z_t}{T_0}\right]^{mg/k\lambda} \exp\left(-\frac{mg(z - z_t)}{k(T_0 - \lambda z_t)}\right), \quad (9)$$

for  $z_t \leq z \leq z_s$ . Plugging this and (2)-(3) in Edlen's formula (1), we get for the troposphere and stratosphere the variation of the refractive index as a function of altitude. As stated before, for altitudes higher than  $z_s$  we can merely use  $n = 1$ . The refractive index profile as a function of altitude calculated in this manner for the parameters of the U.S. Standard Atmosphere is plotted in Fig. 2.

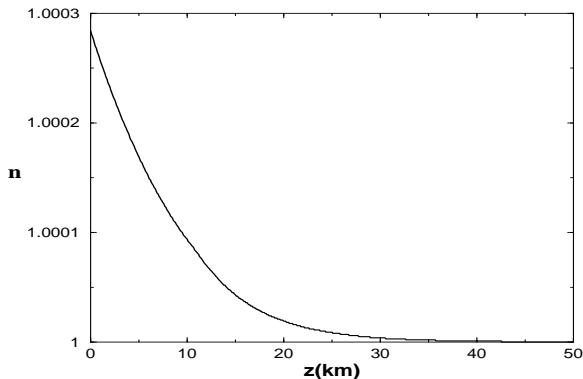


FIG. 2. The used refractive index profile for  $T_0 = 10^0 C$ ,  $P_0 = 1atm$ ,  $\lambda = 6.5K/km$  and  $\nu = 20000cm^{-1}$ .

### III. TRAJECTORY OF A LIGHT-RAY IN THE ATMOSPHERE

We present now three different methods for computing the path of a light-ray in our optical atmosphere model. We proved that the results given by these methods are the same, justifying our forthcoming theoretical considerations. None of these methods is purely analytical, they all make use of numerical calculations to derive the light-ray trajectory. In the following we briefly describe these methods and sketch how one can compute the deviation angle due to atmospheric refraction for light-rays coming from distant sources. In order to avoid the phenomenon of dispersion let us first consider monochromatic light.

### A. The Integral method

This method closely follows the one discussed by Smart [7]. To illustrate the method we use the geometry from Fig. 3.

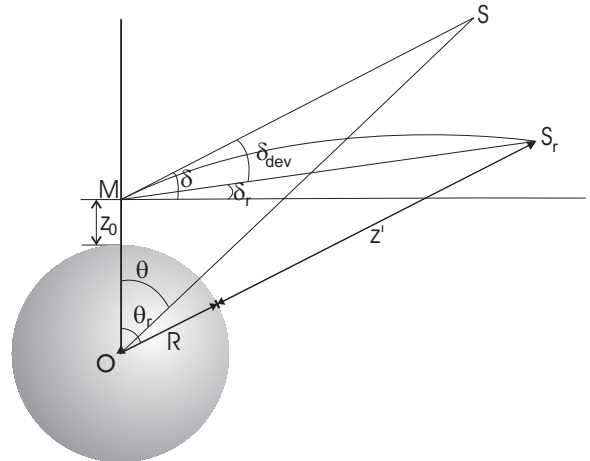


FIG. 3. Real ( $S_r$ ) and apparent ( $S$ ) position of a distant source  $S$ , as observed from the point  $M$  within the Earth's inner atmosphere.

An observer in  $M$  (at altitude  $z_0$ ) detects the light-source placed in  $S_r$  (altitude  $z'$ ). Let the arc  $S_rM$  be the presumed path of the light-ray between the  $S_r$  source and the observer in  $M$ . The observer detects the light ray in the  $MS$  direction, which is tangent to the ray path in  $M$ . The source will be positioned by the observer in  $S$  ( $SO$  and  $S_rO$  have radial directions, thus the light-rays in these directions would not bend within our optical atmosphere model). We denote by  $\delta$  the apparent inclination angle, characterizing the direction of the  $S$  image. Let  $\delta_{dev}$  be the deviation angle of  $MS$  relative to the real  $MS_r$  direction of the source. The meaning of the  $\theta$  and  $\theta_r$  angles are obvious from the figure. We are now interested to compute  $\delta_{dev}$  as a function of  $\delta$ . Presuming that  $z' \gg z_0$  (i.e. the source is very far from the Earth), we can approximate  $MS$ ,  $MS_r$  and  $OS$  by  $z'$ . Some elementary geometry will convince us that the following approximations are justified:

$$\theta \approx \frac{\pi}{2} - \delta - \arcsin\left[\frac{z_0 + R_E}{z' + R_E} \cos \delta\right] \quad (10)$$

$$\delta_{dev} \approx \theta_r - \theta + \frac{R_E + z_0}{R_E + z'} (\sin \theta_r - \sin \theta) \quad (11)$$

In order to get the desired  $\delta_{dev}(\delta)$  dependence we need  $\theta_r$  as a function of  $\delta$ .

Let us follow now a light-ray approaching the Earth and let us consider the atmosphere stratified in infinitesimally thin layers of thickness  $\Delta r$ , with slightly different refractive indices (Fig. 4).

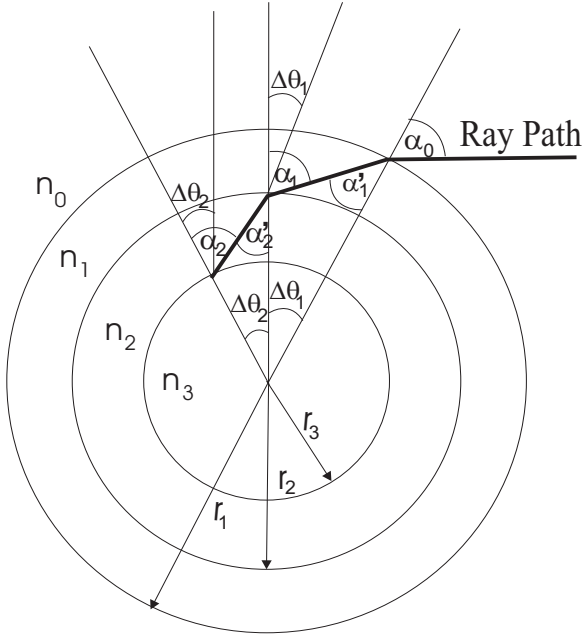


FIG. 4. Trajectory of a light-ray in a layered optical atmosphere model.

A useful relation between the initial incident angle  $\alpha_0$  (in layer with refractive index  $n_0$ ) and a later incident angle  $\alpha_k$  (for a layer with refractive index  $n_k$ ) can be derived. Using Snell's law and the notations from Fig. 4, we can write:

$$\frac{\sin \alpha_0}{\sin \alpha'_1} = \frac{n_1}{n_0} \quad (12)$$

$$\Delta\theta_1 = \alpha_1 - \alpha'_1. \quad (13)$$

This leads to:

$$\sin \alpha_1 = \frac{n_0}{n_1} \sin \alpha_0 (\cos \Delta\theta_1 + \sin \Delta\theta_1 \cot \alpha'_1). \quad (14)$$

Similarly

$$\sin \alpha_2 = \frac{n_1}{n_2} \sin \alpha_1 (\cos \Delta\theta_2 + \sin \Delta\theta_2 \cot \alpha'_2), \quad (15)$$

and combining with (14) it leads to:

$$\sin \alpha_2 = \frac{n_0}{n_2} \sin \alpha_0 (\cos \Delta\theta_1 + \sin \Delta\theta_1 \cot \alpha'_1) \times (\cos \Delta\theta_2 + \sin \Delta\theta_2 \cot \alpha'_2). \quad (16)$$

Generalizing the above equation we get:

$$\sin \alpha_k = \frac{n_0}{n_k} \sin \alpha_0 (\cos \Delta\theta_1 + \sin \Delta\theta_1 \cot \alpha'_1) \times \dots \times (\cos \Delta\theta_k + \sin \Delta\theta_k \cot \alpha'_k). \quad (17)$$

Since the  $\Delta\theta_i$  angles are small, the following approximations are justified:

$$\sin \Delta\theta_i \approx \Delta\theta_i, \quad (18)$$

$$\cos \Delta\theta_i \approx 1, \quad (19)$$

$$\cot \alpha'_i \approx \frac{\Delta r}{r_i \Delta\theta_i}. \quad (20)$$

Using these approximations and the fact that  $\Delta r \ll r_i$  we get:

$$\begin{aligned} \sin \alpha_k &= \frac{n_0}{n_k} \sin \alpha_0 \prod_{i=1}^k (1 + \Delta\theta_i \frac{\Delta r}{r_i \Delta\theta_i}) \approx \\ &\frac{n_0}{n_k} \sin \alpha_0 (1 + \sum_{i=1}^k \frac{\Delta r}{r_i}) \approx \frac{n_0}{n_k} \sin \alpha_0 (1 + \int_{r_k}^{r_0} \frac{dr}{r}) = \\ &\frac{n_0}{n_k} \sin \alpha_0 (1 + \ln \frac{r_0}{r_k}). \end{aligned} \quad (21)$$

Presuming now  $r_0/r_k \approx 1$ , we get:

$$\sin \alpha_k = \frac{r_0 n_0 \sin \alpha_0}{r_k n_k}. \quad (22)$$

Following the geometry from Fig. 4 we get

$$\frac{\Delta r}{r_i} \tan \alpha_i = \frac{\Delta r}{r_i} \frac{1}{\sqrt{\frac{1}{\sin^2 \alpha_i} - 1}}, \quad (23)$$

which in the  $\Delta r \rightarrow 0$  and  $\alpha_i = \alpha(r)$  continuous limit yields:

$$d\theta = \frac{dr}{r} \frac{1}{\sqrt{\frac{1}{\sin^2 \alpha(r)} - 1}}. \quad (24)$$

Denoting by  $\alpha_M$  the final incident angle at the observer and using (22) we get:

$$d\theta = \frac{dr}{r} \frac{1}{\sqrt{\left[\frac{n(r)}{n(r_M)}\right]^2 \frac{1}{\sin^2 \alpha_M} \frac{r}{r_M} - 1}}. \quad (25)$$

By using the fact that  $\sin^2 \alpha_M = \cos^2 \delta$  we can finally determine the angle  $\theta_r$  as a function of  $\delta$  by integrating (25):

$$\theta_r = \int_{z_0+R_E}^{z'+R_E} \frac{dz}{\sqrt{\left[\frac{n(z)}{n(z_0)}\right]^2 \frac{1}{\cos^2 \delta} \frac{z+R_E}{z_0+R_E} - 1}}. \quad (26)$$

The above integral can be only numerically computed. There is of course a singularity at  $z = z_0$ , which can be eliminated by a Gauss-Chebisev expansion, or by adjusting the step in the numerical integration in the vicinity of the singularity (the method followed by us). Computing numerically  $\theta_r$  as a function of  $\delta$  and by getting from (10)  $\theta$  as a function of  $\delta$ , we are able now to calculate from (11) the desired  $\delta_{dev}(\delta)$  dependence.

It is important to mention here that applying the method for  $\delta < 0$  is not straightforward. One must first find in this case the closest point  $C$  of the light-ray trajectory relative to the Earth's surface. This can be done by using the fact that the trajectory is symmetric in the vicinity of this point. Then, we decompose the trajectory in two parts, the first part is from  $M$  to  $C$ , and the second from  $C$  to  $S_r$ . The light-ray can be followed now by the presented methods both on the  $CS_r$  and  $CM$  segments. The deviation angle can be also computed.

## B. Using the Fermat principle

The Fermat principle states that light travels between two point along that path which requires the least time, as compared to other nearby paths. We can of course reformulate the Fermat principle by using the optical path instead of time. If the trajectory of a light-ray travelling in the  $X-O-Y$  plane is described by the  $y = y(x)$  curve (see the geometry in Fig. 5), we have that:

$$s = \int_{P_{ini}(x_0, y_0)}^{P_{fin}(x_f, y_f)} n[x, y(x)] ds = \int_{x_0}^{x_f} n[x, y(x)] \sqrt{1 + y'(x)^2} dx, \quad (27)$$

should have a local minima. In the above formula  $n[x, y(x)]$  denotes the refractive index of the medium in point with coordinates  $x, y(x)$ . In our case  $n$  has a spherical symmetry, depending on the  $z = \sqrt{x^2 + y(x)^2} - R_E$  altitude only.

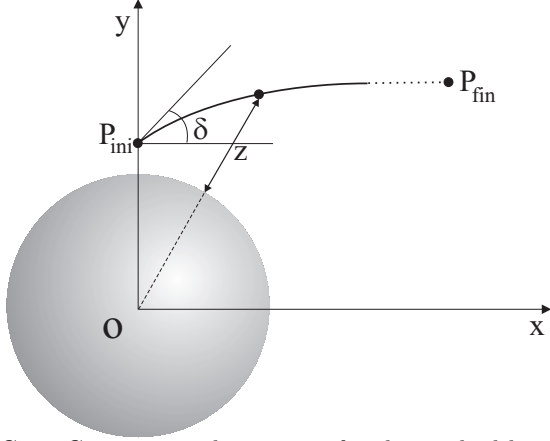


FIG. 5. Geometry and notations for the method based on the Fermat principle.

One can write then (27) as:

$$s = \int_{x_0}^{x_f} f[x, y(x), y'(x)] dx, \quad (28)$$

with:

$$f[x, y(x), y'(x)] = n[\sqrt{x^2 + y(x)^2} - R_E] \sqrt{1 + y'(x)^2}. \quad (29)$$

We are looking now for the  $y(x)$  function that minimizes  $s$ . If we fix the two points  $P_{ini}$  and  $P_{fin}$  between which the light travels, the minima of  $s$  leads to a classical variational problem

$$\delta s = 0, \quad (30)$$

with:

$$\delta[y(x)]|_{x=x_0} = 0, \quad (31)$$

$$\delta[y(x)]|_{x=x_f} = 0. \quad (32)$$

The solution of this problem is well-known [8], and given by the second-order differential equation:

$$\frac{\partial f}{\partial y} - \frac{d}{dx} \left[ \frac{\partial f}{\partial y'} \right] = 0. \quad (33)$$

It is straightforward to show that:

$$\frac{\partial f}{\partial y} = \frac{\partial n}{\partial z} [x, y(x)] \frac{y(x)}{\sqrt{y^2(x) + x^2}} \sqrt{1 + y'(x)^2}, \quad (34)$$

$$\frac{d}{dx} \left[ \frac{\partial f}{\partial y'} \right] = \frac{\partial n}{\partial z} [x, y(x)] \frac{y'(x)y(x) + x}{\sqrt{y(x)^2 + x^2}} \times \frac{y'(x)}{\sqrt{1 + y'(x)^2}} + n[x, y(x)] y''(x) \frac{1}{[1 + y'(x)^2]^{3/2}} \quad (35)$$

By simple algebra we obtain from this a second-order differential equation for the  $y(x)$  equation describing the trajectory of the light-ray:

$$y''(x) = \frac{\partial n}{\partial z} [x, y(x)] \frac{[1 + y'(x)^2]}{n[x, y(x)] \sqrt{x^2 + y(x)^2}} \times \{y(x)[1 + y'(x)^2] - y'(x)[y(x)y'(x) + x]\}. \quad (36)$$

Taking the  $n(z)$  refractive index profile from our optical atmosphere model, equation (36) can be numerically integrated. We start from a  $P_{ini}(x_0, y_0)$  point and consider a  $\tan \delta = y'(x_0)$  initial derivative. The angle  $\delta$  will be the apparent inclination angle of the light-ray in  $P_{ini}$  (the point where the observer is presumed). The  $y(x)$  trajectory can be computed by numerically integrating (36) with the  $y(x_0) = y_0$  and  $y'(x_0) = \tan \delta$  initial conditions. We construct thus the  $y(x)$  trajectory from point-to-point, up to an altitude  $z \geq z_s$ , where  $n(z) = 1$  can be presumed. The derivative of  $y(x)$  at this point will determine the  $\delta_r$  angle of the light-ray at the border of the optical atmosphere. For altitudes higher than this, the trajectory of the light-ray is presumed rectilinear. The deviation angle is then simply approximated as  $\delta_{dev} = \delta - \delta_r$ , and the desired  $\delta(\delta_{dev})$  dependence can be numerically computed.

## C. The simulation method

As its name suggests this is simply a computer simulation method in which we follow the light-ray by segments of infinitesimally small and fixed-length lines. The angle between two elementary line is given by estimating the refractive index at their end-points and by using Snell's law. The trajectory of the light-ray is then constructed starting from the observer with an initial angle  $\delta$ , and computing the ray-path from point-to-point until it leaves the optical atmosphere and the refractive index can be taken as 1. At this point the direction of the

light-ray determines the final angle  $\delta_r$ , and the deviation is computed as  $\delta_{dev} = \delta - \delta_r$ . Resembling the method based on the Fermat principle, this simulation also works smoothly for arbitrary positive or negative  $\delta$  values. Due to the fact that for an elementary step the changes in the refractive index is rather small, it is crucial to work with the maximal precision offered by the computing environment.

We mention here that all three methods give identical results, proving their applicability and our theoretical considerations. As an example, for the parameters of the U.S. Standard Atmosphere, results for the  $\delta_{dev}$  deviation angle versus the apparent inclination angle,  $\delta$ , is plotted on Fig.6 ( $T_0 = 10^0C$ ,  $P_0 = 1atm = 101.3kPa$ ,  $\nu = 20000cm^{-1}$  wave-number for the light and  $\lambda = 6.5K/km$  lapse-rate).

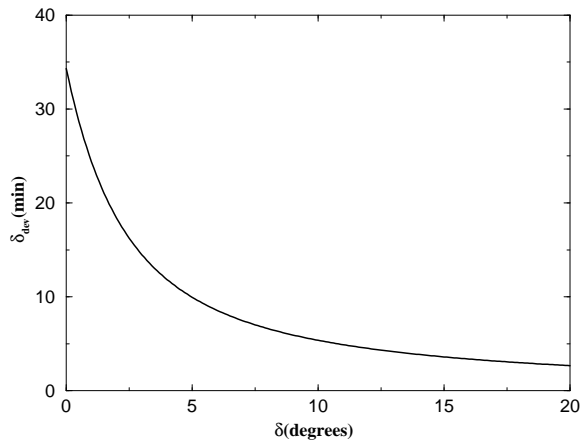


FIG. 6. Deviation angle  $\delta_{dev}$  between the apparent and real location of a point-like source far from Earth as a function of the  $\delta$  apparent inclination angle. ( $T_0 = 10^0C$ ,  $P_0 = 1atm$ , standard  $\lambda = 6.5K/km$  lapse-rate and observation from sea-level)

These results are in excellent agreement with the one given by Thomas and Joseph [4] and the report of the U.S. Naval Observatory (1993) [9]. From Fig. 6 we learn that the deviation angle is usually quite small, and becomes important only when viewing objects in the vicinity of the optical horizon. The deviation angle increases sharply for very small inclination angles. This effect is responsible for the flattened shape of the rising (or setting) Sun and Moon, and also for the fact that these heavenly objects appear more flattened at their bottom. It is also interesting to note here that the angular extent of the Sun and full-Moon is 32 arcmin, and the maximum deviation obtained for standard conditions is 34.5 arcmin. This leads us to the observation that the Sun or Moon is visible even when in reality it is below the geometrical horizon.

#### IV. COMPUTING THE FLATNESS

Once we numerically determined the  $\delta_{dev}$  deviation angle as a function of the  $\delta$  apparent inclination angle, it is easy to characterize the apparently flat rim of the setting Sun. Atmospheric refraction influences only the  $\Delta_v$  vertical angular extent of the Sun (or Moon), which becomes thus smaller than the  $\Delta_h$  horizontal extent. The asymmetry ratio (or the flatness) for the rim of the Sun can be described by the

$$\alpha = \frac{\Delta_h}{\Delta_v}, \quad (37)$$

ratio (of course  $\alpha \in [1, \infty)$ ). Since both the Sun and the full-Moon are normally visible under a  $\Delta_0 = 32 \text{ arcmin}$  angular extent, we have  $\Delta_h = \Delta_0$ . The value of  $\Delta_v$  can be derived after numerically computing the  $\delta$  apparent inclination angle as a function of the  $\delta_r = \delta + \delta_{dev}$  real inclination, i.e.  $\delta = F(\delta_r)$ . If the apparent inclination angle for the bottom of the Sun is  $\delta_0$ , corresponding to a  $\delta_{r0}$  real inclination angle, than

$$\Delta_v(\delta_0) = F(\delta_{r0} + \Delta_0) - \delta_0, \quad (38)$$

and we get:

$$\alpha(\delta_0) = \frac{\Delta_0}{F(\delta_{r0} + \Delta_0) - \delta_0} \quad (39)$$

For fixed observation altitude and meteorological conditions the  $\alpha_c$  maximal possible flatness corresponds to the situation when the bottom of the Sun touches the horizon. This happens for a  $\delta_0 = \delta_c$  critical inclination angle.

By decreasing the  $\delta$  angle in small steps, and applying the previously described methods for computing the light-ray trajectory, both the  $\delta = F(\delta_r)$  function and  $\delta_c$  is numerically determined. In our calculations we have chosen to decrease  $\delta$  in steps of  $0.01^0$ .

#### V. RESULTS

Applying the methods presented in the previous sections and our optical atmosphere model, we systematically computed the  $\alpha_c$  asymmetry ratio for the rim of the setting Sun as a function of observational altitude and meteorological conditions parameterized by pressure and temperature. We have also shown that the value of  $\alpha$  is insensitive to details of the considered optical atmosphere model, proving the stability of our results. In the following we detail our findings. For all the calculations we considered monochromatic light with wave-number of  $\nu = 20000cm^{-1}$ , corresponding to the green color. If otherwise not specified we considered the height of the troposphere  $z_t = 14km$  and the height of the stratosphere as  $z_s = 50km$ .

### A. Stability regarding the considered optical atmosphere model

As discussed in section II., for the construction of the refractive index profile we borrowed results from the U.S. Standard Atmosphere model. The main parameters needed by us is the  $z_t$  height of the troposphere, the  $z_s$  height of the stratosphere and the  $\lambda$  lapse-rate.

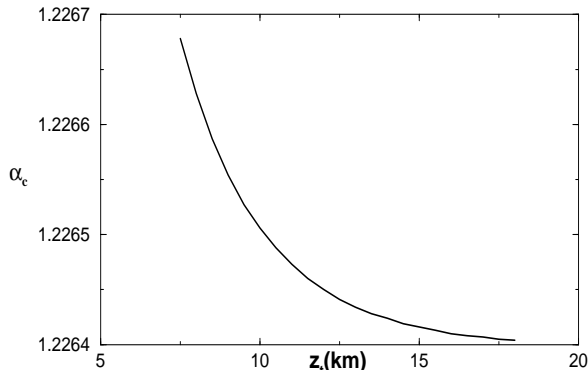


FIG. 7. Maximal observable flatness,  $\alpha_c$  as a function of the  $z_t$  height of the troposphere. ( $T_0 = 0^0C$ ,  $P_0 = 1atm$ , normal lapse-rate and observation from sea-level)

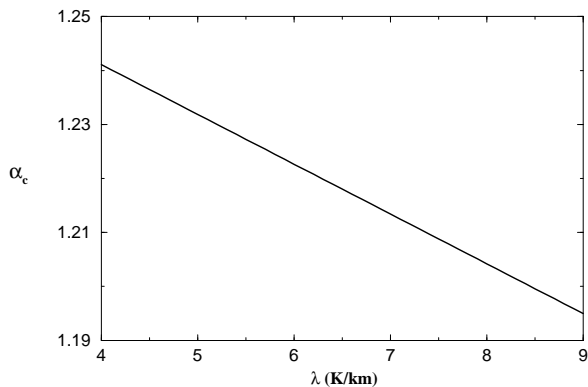


FIG. 8. Maximal observable flatness,  $\alpha_c$  as a function of the  $\lambda$  lapse-rate in the troposphere. ( $T_0 = 0^0C$ ,  $P_0 = 1atm$ , and observation from sea-level)

It is evident, that the exact value of  $z_s$  does not much influence our results, since in the stratosphere the refractive index is already very close to 1. As a first step we studied thus the influence of  $z_t$  on the  $\alpha_c$  asymmetry ratio. We considered normal conditions with  $T_0 = 0^0C$ ,  $P_0 = 1atm$ , observations at sea-level ( $z_0 = 0$ ) and  $\lambda = 6.5K/km$  standard lapse-rate. As illustrated on Fig. 7, the value of  $z_t$  (in a reasonable range) has no significant influence (note the scale on the vertical axis). The value of the lapse-rate has already a more noticeable effect on  $\alpha_c$  (Fig. 8), however this variation is also quite small for the practically important fluctuations around the standard  $\lambda = 6.5K/km$  value. We conclude thus, that our results are quite stable regarding the details of

the considered optical atmosphere model.

### B. Asymmetry as a function of the inclination angle

We computed the observable  $\alpha$  flatness as function of the apparent inclination angle of the Sun's bottom. Results for  $T_0 = 0^0C$ ,  $P_0 = 1atm = 101.3kPa$ ,  $\lambda = 6.5K/km$  and observations at sea-level are presented on Fig. 9. As emphasized before, the asymmetric rim of the setting (or rising) Sun becomes evident only for very small  $\delta_0$  values, when the Sun is close to the horizon. For these normal parameters we get that  $\alpha_c$  is around 1.2.

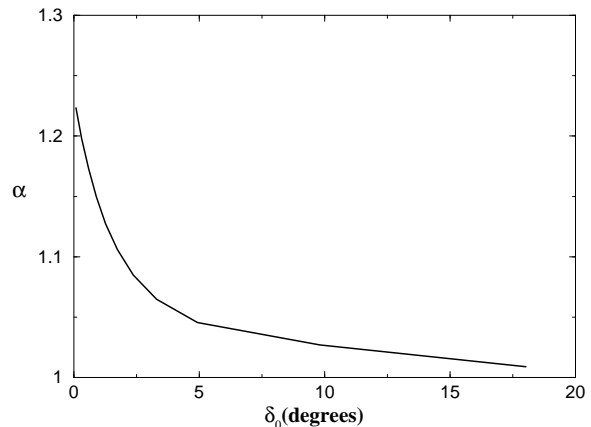


FIG. 9. Observable flatness,  $\alpha$ , as a function of the  $\delta_0$  inclination angle of the bottom of the Sun. ( $T_0 = 0^0C$ ,  $P_0 = 1atm$ , observation from sea-level and standard lapse-rate)

### C. Flatness as a function of observation height

Let us presume now that the observer is at height  $z_0$  above the sea-level, and there is no obstacle in the direction of the horizon, which is at sea-level (i.e. we are above a vast ocean). It is obvious that from higher altitude the  $\delta_c$  critical angle will be smaller (becomes negative) and the deviation angle increases more sharply in the neighborhood of  $\delta_c$ . This leads us immediately to the conjecture that the observed flatness should be larger. Taking the  $T_0 = 0^0C$  and  $P_0 = 1atm$  normal atmospheric conditions at sea-level, the standard  $\lambda = 6.5K/km$ , lapse-rate we can compute the  $\alpha_c$  maximal observable flatness as a function of observation height. Results in this sense are plotted in Fig. 10. As expected,  $\alpha_c$  increases with  $z_0$ . For these normal conditions we get that from the top of a  $5km$  height mountain we would observe an  $\alpha_c \approx 1.5$  flatness and from a commercial flight at  $10km$  height at sunset we would detect an  $\alpha_c \approx 1.7$  maximal flatness. For altitudes above  $30km$ , or observations made from a space-shuttle we can get extreme values for  $\alpha_c$  up to 2.5.

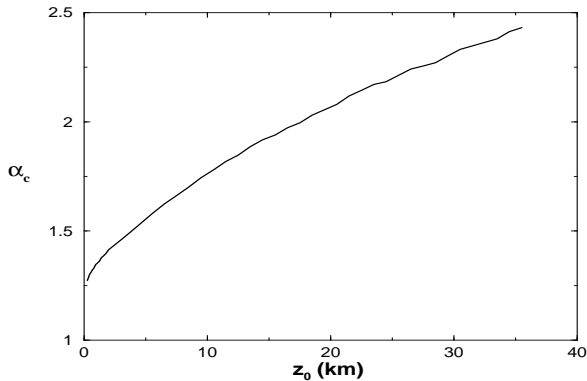


FIG. 10. Maximal observable flatness,  $\alpha_c$  as a function of the  $z_0$  observation height. ( $T_0 = 0^{\circ}C$ ,  $P_0 = 1atm$  and standard  $\lambda = 6.5K/km$  lapse-rate)

#### D. Influence of temperature

The  $T_0$  temperature measured at sea-level influences in an important manner the observed flatness. Computing the temperature dependence of  $\alpha_c$  for observations at sea-level, normal  $P_0 = 1atm$  atmospheric pressure and standard lapse-rate we get the values presented in Fig. 11. While for a  $T_0 = 30^{\circ}C$  temperature  $\alpha_c$  is around 1.1 for  $T_0 = -40^{\circ}C$  it becomes 1.3, and increases more and more sharply for lower temperatures (arctic conditions).

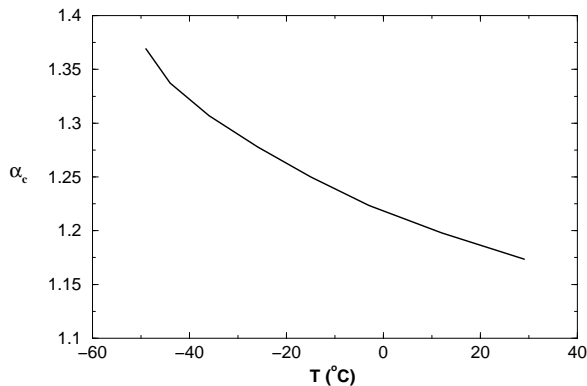


FIG. 11. Maximal observable flatness,  $\alpha_c$  as a function of the air temperature measured at sea-level. ( $P_0 = 1atm$ , observations at sea-level and standard  $\lambda = 6.5K/km$  lapse-rate)

#### E. Influence of atmospheric pressure

Increasing the  $P_0$  pressure at sea-level results the increase of the observable  $\alpha_c$  flatness. For the reasonable and measurable  $P_0$  values,  $T_0 = 0^{\circ}C$ , observation at sea-level and standard lapse-rate the variation is almost linear (Fig.12). For an extreme  $P_0 = 125kPa$  pressure one can detect an asymmetry ratio of 1.3.

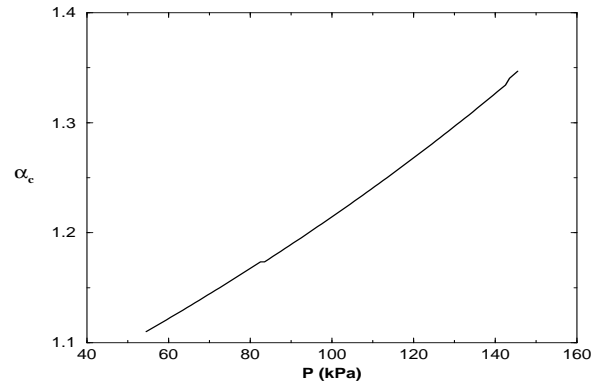


FIG. 12. Maximal observable flatness,  $\alpha_c$  as a function of the atmospheric pressure at sea-level. ( $T_0 = 0^{\circ}C$ , observation at sea-level and standard  $\lambda = 6.5K/km$  lapse-rate)

## VI. EXPERIMENTS

By simple experiments it is relatively easy to measure the flatness of the setting (or rising) Sun. We considered photo and video experiments, and analyzed the pictures as a function of the inclination angle of the Sun. With an appropriate filter and calibrated eye-piece, telescope observations were also possible. In order to obtain usable pictures with a nicely visible rim we had to ensure a properly adjusted light intensity. Appropriate filters, specific atmospheric conditions and usually small  $\delta_0$  inclination angles lead us to usable pictures. When the Sun is close to the horizon, the inclination angle of the Sun can be directly determined by analyzing the taken picture. We can use the fact that the horizontal angular extent of the Sun always corresponds to  $32arcmin$ . The distance of the Sun from the horizon can then be compared with the horizontal extent of the setting Sun and the inclination angle results directly from the picture. Making experiments with the setting or rising Moon is more complicated, since one needs a full-Moon for this, a work during the night and we have to deal with pictures where the horizon is not clearly visible.

First, we have taken several series of pictures in South-Bend (Indiana, altitude  $100m$ ) both in winter and late-spring, studying very different temperature conditions. As an immediate confirmation of our theoretical results, from these pictures it was obvious that for the same inclination angle the flatness is bigger in winter, i.e. for lower  $T_0$  values. Two series of digitized and appropriately enhanced pictures are visible on the web-page dedicated to this study [10]. Results from these pictures, in comparison with the expected (computed) flatness is presented on Fig. 13. The first set of pictures is a sunrise in winter. The mean temperature during the sunrise was  $-5^{\circ}C$ , and the atmospheric pressure was  $103kPa$ . It is important to note that during this sunrise the temperature remained approximately constant. The second set of picture was made in late-spring for a sunset. During this sunset the mean-temperature was  $12^{\circ}C$ , the atmospheric pressure

98kPa and the temperature dropped detectably during the time the pictures were made. Results for the flatness as a function of the Sun's inclination angle (bottom of the rim) is plotted with filled circles and triangles for the winter and spring series, respectively.

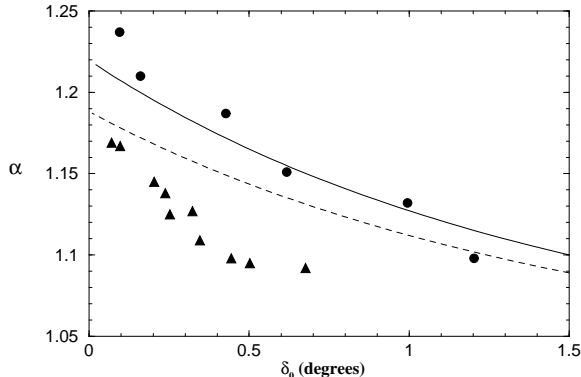


FIG. 13. Flatness as a function of inclination angle. Comparison between experimental results and theory for a sunrise and a sunset photo sequence. Filled circles are results from sunrise pictures taken in winter with  $T_0 = -5^{\circ}C$  and  $P_0 = 103kPa$ . Filled triangles correspond for pictures taken in May with  $\langle T_0 \rangle = 12^{\circ}C$  and  $P_0 = 98kPa$ . Observations were made at  $z_0 = 100m$  height with the horizon roughly at the same altitude. Theoretical results for the corresponding atmospheric conditions and  $\lambda = 6.5K/km$  standard lapse-rate is plotted by continuous and dashed lines for the winter and spring conditions, respectively.

The theoretical curves were constructed for the mentioned mean temperature, pressure, observation height of 100m with the horizon at the same altitude and a standard lapse-rate. These results are plotted on Fig. 13 by a continuous and dashed line for the winter and spring conditions, respectively. As observable from Fig. 13 for the winter conditions the measured  $\alpha$  values are in acceptable agreement with the one given by our theory. However, for the spring series the expected  $\alpha$  values are higher, and decreasing slower as a function of the  $\delta_0$  inclination angle, than the measured data. A reason to account for this sharper trend is the decreasing temperature measured during the sunset. Taking this effect into account in the calculations, would definitely result in a trend closer to the observed one. This temperature variation does not account however, for the constantly lower values measured for  $\alpha$ . The only arguments we can give in this sense is that probably the atmosphere at the time of this measurement had a refractive index profile different from the one proposed in our model, behaving in a non-standard manner.

A second set of experiments were realized by video-filming sunsets in Cluj (Romania). The obtained continuous set of picture allowed us to follow-up more precisely the flatness as a function of the inclination angle. The inclination angle was calculated from the images by the same method as in photographs, i.e. by comparing the

height between the bottom of the Sun and horizon with the horizontal extent of the setting Sun. Since Cluj is not a flat region like South-Bend, we had to be careful in choosing the observation point, and to determine also the altitude of the optical horizon. Results from video-recording in comparison with theoretical expectations (corresponding to the appropriate atmospheric conditions) are plotted in Fig. 14. For this measurement a quite fair agreement between theoretical and experimental data is achieved. Since the lapse-rate for the theoretical prediction was taken from the standard atmosphere model, the slightly greater  $\alpha$  values calculated by us are explainable.

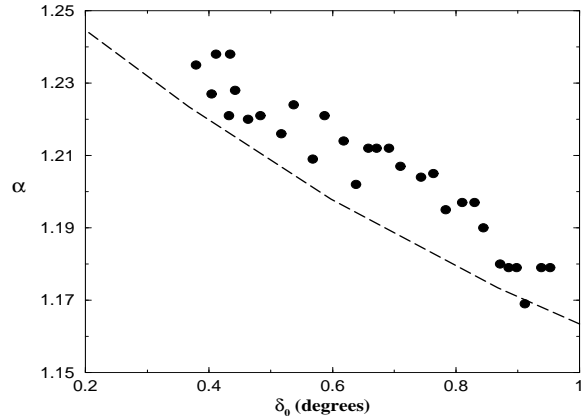


FIG. 14. Experimental (dots) and theoretical results (dashed line) for the flatness as a function of the inclination angle from a sunset video-recording. ( $T_0 = 7^{\circ}C$   $P_0 = 108kPa$ , observation at  $z_0 = 400m$ , horizon at  $z_0 = 300m$  and a presumed standard  $\lambda = 6.5K/km$  lapse-rate)

## VII. PICTURES AND MOVIES FROM THE INTERNET

Sunset or sunrise (moon-set or moon-rise) is usually a spectacular phenomena, and thus it is a favorite theme for professional and amateur photographers. The Internet is full of beautiful and useful pictures in this sense. Many of these pictures are taken in extreme conditions (arctic environment, airplanes, space-shuttle or high mountains), offering us an excellent possibility to check our calculations under these conditions, too. Moreover, on the web there are also interesting, freely downloadable or public domain movies exemplifying how the observed flatness increases in the neighborhood of the horizon.

We performed an extensive search on the Internet and collected non-copyrighted materials about sunset, sunrise, moon-set and moon-rise. Since their presentation in the context of this paper is impossible we classified and stored them on the web-page [10] dedicated to this study. The interested reader can browse this collection and convince himself or herself that these pictures support our theoretical results for the estimated flatness. In

agreement with our expectations we found that for a sunrise (or sunset) viewed from a space-shuttle  $\alpha_c$  should be of the order 2 – 2.5, and in arctic environment  $\alpha_c$  increases up to values of 1.3. For most of the everyday, usual and low-altitude photos one finds  $\alpha_c \approx 1.1 - 1.2$ . Pictures taken from commercial airplane yield  $\alpha_c \approx 1.5$ . We also found a picture-series for a sunset over the ocean, where the rim of the Sun is nicely visible. The scenario presented in this photo is again in agreement with our theoretical predictions.

The movies stored on our web-page will also convince the reader about the sharp variation of  $\alpha$  as a function of the  $\delta_0$  deviation angle. A public domain movie, showing a moon-set viewed from the space-shuttle illustrates observations from high altitudes.

### VIII. THE GREEN FLASH

Although the explanation and the study of the green flash is not the aim of the present paper, we briefly discuss here how this phenomenon can be understood and studied through our methods.

From equation (1) it is obvious that atmospheric refraction depends on the frequency (color) of the light-ray, a phenomenon called dispersion. Differently colored light-rays coming from a source emitting a continuous spectra will suffer different deviations. More strongly will bend the light-rays with bigger frequencies, leading to a separation of the colors in the observed Sun. Since the high-frequency visible components (corresponding to violet and blue colors) are strongly scattered by the atmosphere, the green component reaching directly the observer will suffer the strongest bending. When the Sun disappears below the horizon this component will be observed lastly, leading to a green-flash on the horizon. Since for standard atmospheric conditions the dispersion from atmospheric refraction is tinny, the effect is hardly observable for usual and everyday conditions. Green flashes become observable exactly under those conditions under which the flatness is more accentuated. This means high observation altitudes, low temperature and high pressure. As an illustration of this, we have just learned that for airplane pilots it is a quite usual phenomenon. Green flashes are often seen in non-standard optical atmosphere, when mirages appear. This is generally the case when layers of air with strongly different temperatures are in contact.

For a nice presentation and discussion on green flashes the interested reader should consult the excellent homepage of A.T. Young [3].

### IX. SUNSET SIMULATION PROGRAM

We also created a computer-code which simulates the sunset on the computer-screen. By using the discussed

simulation method, the program computes and visualizes the rim of the Sun during a sunset. After fixing the atmospheric conditions (temperature and pressure) and observation height in the menu, one can follow up how a sunset might look like in our optical atmosphere. The program runs under Windows environment and one can freely download the executable from the web-page accompanying this study [10].

### X. CONCLUSIONS

Atmospheric refraction is responsible for the asymmetric rim of the setting (or rising) Sun. Three different methods yielding the same results were presented here to compute the path of a light-ray in an optical atmosphere model, where the refraction index varies continuously as a function of altitude. By determining the deviation angle between the apparent and real inclination of a point-like light-source which is at a large distance from the Earth, we were able to compute the  $\alpha$  asymmetry ratio for the rim of the setting Sun. We investigated  $\alpha$  as a function of the inclination angle, observation altitude and atmospheric conditions. We found that the maximal flatness obtained in the vicinity of the horizon increases as a function of observation altitude and pressure, and decreases as the temperature increases. We found that  $\alpha$  is rather insensitive to the fine-details of the considered optical atmosphere model, which makes our results robust. The maximal flatness observable under normal conditions at sea-level is around 1.2. At extremely low temperatures ( $-40^{\circ}C$ ) one can observe values up to 1.3 and for high altitude observations (space-shuttle) one can get an asymmetry ratio of 2.5. By simple experiments and pictures from the Internet we illustrate and prove our theoretical predictions. The methods presented here can be effectively used to study atmospheric refractions in non-standard atmospheric conditions as well. In this manner one can study mirages or the green flash phenomenon. A freeware computer program created by us and downloadable from the web-page accompanying this study simulates the sunset for arbitrary atmospheric conditions and observation altitude.

### XI. ACKNOWLEDGMENTS

We thank the Bergen Computational Physics Laboratory in the framework of the European Community - Access to Research Infrastructure of the Improving Human Potential programme for access to their supercomputer facilities. The work of Z. Neda was sponsored by the Sapientia foundation. We thank I. Albert and T. Néda for useful discussions and help in the video and photo experiments.

- [1] <http://mintaka.sdsu.edu/GF/bibliog/bibliog.html>
- [2] Aristotle, "Meteorologica, with an English translation by H.D.P. Lee" (Harvard University Press, Cambridge, 1962)
- [3] <http://mintaka.sdsu.edu/GF/index.html>
- [4] M.E. Thomas and R.I. Joseph, "Astronomical Refraction", John Hopkins APL Technical Digest **7** (3) 279-284 (1996)
- [5] B. Edlen, "The Refractive Index of Air", Meteorologia **2** 71-80 (1966)
- [6] U.S. Standard Atmosphere 1976 (U.S. Government Printing Office, Washington D.C., 1976)
- [7] W. M. Smart, "Spherical Astronomy" (6th Ed., Cambridge University Press, Cambridge, 1977)
- [8] G.B. Arfken and H.J. Weber, "Mathematical Methods for Physicists", Chapter 17 (Fourth Edition, Academic Press, London, 1995)
- [9] U.S. Naval Observatory, The Nautical Almanac (U.S. Government Printing Office, Washington D.C., 1993)
- [10] <http://www.fi.uib.no/~neda/sunset/index.html>